Climate Dynamics (2024) 62:2735–2753
https://doi.org/10.1007/s00382-024-07112-6

ORIGINAL ARTICLE

A sub-monthly timescale causality between snow cover and surface air temperature in the Northern Hemisphere inferred by Liang–Kleeman information flow analysis

Yuhei Takaya[1] · Kensuke K. Komatsu[2] · Naresh Govind Ganeshi[1,3] · Takahiro Toyoda[1] · Hiroyasu Hasumi[3]

Received: 28 July 2023 / Accepted: 10 January 2024 / Published online: 1 March 2024

Abstract
Land snow is considered one of the important Earth system elements altering sub-seasonal to seasonal (S2S) atmospheric variability and predictability. However, the causal relationship in the snow–atmosphere interaction and its impact on S2S predictability are still not clearly understood. In this study, we investigated the sub-monthly causal relationship between observed snow cover (SC) and surface air temperature (SAT) in the Northern Hemisphere. We used Liang–Kleeman information flow analysis to scrutinise the direction of causation and identify "cold spots" where SC conditions actively influence SAT on a sub-monthly timescale. The cold spots were identified by geographical location and season: North Eurasia in September and October; East Siberia in October and May; Canada in November; East Asia in November and March; Central Asia in October and November; and East Europe in March. Results based on snow water equivalent instead of SC also confirmed the cold spots identified in SC. Furthermore, we evaluated the SC–SAT causal relation in operational S2S prediction models. The results indicated that the S2S models underestimate the SC influence on SAT to greater or lesser degrees, implying the deficiencies in the models. This study emphasises the importance of faithfully reproducing the SC effect on SAT in S2S models for further possible improvements in sub-seasonal prediction skill. The findings renew a fundamental understanding of the snow–atmosphere interaction and sub-seasonal predictability arising from land snow conditions.

Keywords Land–atmosphere interaction · Snow cover · Sub-seasonal prediction · Causality analysis

1 Introduction

An annual average of the snow cover extent is approximately 24 million km^2, with a maximum of 47 million km^2—roughly half of the total land area in the Northern Hemisphere—in January (Estilow et al. 2015). Thus, land snow is an integral part of land conditions for considering lower-boundary impacts on weather and climate in the Northern Hemisphere (Henderson et al. 2018). Numerous previous studies have suggested various mechanisms involved in the atmosphere–snow–ground thermal interaction: the snow albedo effect (Flanner et al. 2011, Xu and Dirmeyer 2013), snow hydrological effect (Ambadan et al. 2018; Xu and Dirmeyer 2013; Yasunari et al. 1991), snow insulation effect (Cook et al. 2008; Zhang 2005), and snowmelt heat sink (Cohen and Rind 1991). Land snow is considered an important contributor to S2S predictability and, as a proof of concept, model sensitivity experiments have been performed using climate models (Ambadan et al. 2018; Douville 2010; Jeong et al. 2013; Li et al. 2019; Orsolini et al. 2013; Peings et al. 2011; Thomas et al. 2016; Xu and Dirmeyer 2011; Xu and Dirmeyer 2013). Moreover, several possible remote influences of the snow on the atmospheric circulation have been proposed, thus its impacts on the S2S predictability originating from the snow in both local and remote regions have been anticipated, albeit some remote influence in the upper troposphere is still unresolved particularly in modelling studies (Cohen

✉ Yuhei Takaya
yuhei.takaya@mri-jma.go.jp

[1] Meteorological Research Institute, Japan Meteorological Agency, Tsukuba, Japan

[2] Osaka Regional Headquarters, Japan Meteorological Agency, Osaka, Japan

[3] Atmosphere and Ocean Research Institute, The University of Tokyo, Kashiwa, Japan

and Entekhabi 1999; Diro and Lin 2020; Henderson et al. 2018; Jeong et al. 2013; Li et al. 2019; Orsolini et al. 2013, 2016; Kumar and Yang 2003; Ruggieri et al. 2022; Wu and Kirtman 2007).

Regarding the representation of snow processes in models, substantial effort has been made to improve snow processes, and snow–atmosphere interaction in S2S prediction models, along with the snow initialization (e.g., Arduini et al. 2019; Dutra et al. 2010; de Rosney et al. 2014; Gichamo et al. 2022; Lin et al. 2016; Pullen et al. 2011; Saha et al. 2017; Walter et al. 2019). Nevertheless, the snow–atmosphere interaction is still not represented accurately in numerical models (Diro and Lin 2020; Kolstad 2017; Li et al. 2020; Xue et al. 2021). Thus, more efforts in model evaluation and model development based on the evaluation are required for a deeper understanding and improving the model representation of the snow–atmosphere interaction.

Despite the tremendous effort mentioned above, a complete understanding of snow cover influence on S2S atmospheric variability and predictability in the observations and models is still lacking. In particular, the evaluation of models participating in the World Weather Research Programme (WWRP)/World Climate Research Programme (WCRP) Subseasonal to Seasonal Prediction (S2S) Project (Vitart et al. 2017) has not been performed in terms of the snow influence on surface air temperature (SAT; 2-m air temperature). Recently, Diro and Lin (2020) assessed the sub-seasonal prediction skill of snow water equivalent (SWE) and SWE–SAT coupling in models participating in the Subseasonal Prediction Experiment (SubX; Pegion et al. 2019) and provided valuable implications for the sub-seasonal SAT prediction skill. They suggested that the underestimated snow–SAT coupling in the Environment and Climate Change Canada's Global Ensemble Prediction System (ECCC-GEPS; Lin et al. 2016) is one of the factors for lowering sub-seasonal SAT prediction skill. On the other hand, for a better understanding of the origins of predictability, it is necessary to separate cause and effect involved in the snow–atmosphere interaction (Kolstad 2017; Komatsu et al. 2023). Existing conventional approaches such as correlation analysis have limitations in uncovering the causal relationship between snow and atmospheric variabilities due to their long memory. That is, although simultaneous correlation and regression analysis can find a statistical linear association between variables (e.g., Diro and Lin 2020), it cannot infer the direction of causation. A lagged correlation or lagged composite analysis may provide information on the causation, however, they fail to reveal the causality if the long memory exists in the variables analysed (McGraw and Bernes 2018). Due to the complexity and the memory effects of the land, disentangling the causality in the land–atmosphere interaction through statistical analysis is often challenging.

An alternative approach for uncovering the causality is conducting sensitivity experiments using climate models. Usually, a pair of sensitivity experiments are conducted by either changing initial land conditions or restoring the land variables to the climatological mean or realistic conditions during model integrations (e.g., Ardilouze et al. 2017; Douville 2010; Dutra et al. 2011; Jeong et al. 2013; Koster et al. 2011; Peings et al. 2011; Thomas et al. 2016). Jeong et al. (2013), by performing extensive sensitivity experiments, provided a comprehensive view of snow initialization impacts on sub-seasonal SAT prediction during the whole cold season, which implies the causation in the snow–atmosphere interaction. The model experiment approaches can quantify the influence of the snow conditions on the atmosphere to some extent but also have some shortcomings. First, it is impossible to compare the land influence assessed by the sensitivity experiments with an observational counterpart. Second, the estimates of the coupling strength depend on the model used. Third, these approaches may disturb the land–atmosphere interaction by intervening physical processes in models because imposed land conditions are not physically balanced. Fourth, a large amount of climate model integration required for the sensitivity experiments hinder inter-model comparisons to investigate differences in snow effects between different models.

To complement the above-mentioned modelling approaches for assessing the causality and impacts, this study uses a tractable novel technique called Liang–Kleeman information flow, which has been devised based on the information theory and is a rigorous form of approximate transfer entropy (Liang and Kleeman 2005; Liang 2014, 2015). The Liang–Kleeman information flow can evaluate cause and effect in dynamical systems. The technique has been successfully applied to numerous problems in various disciplines and has recently spurred in climate research as well (Bai et al. 2018; Docquier et al. 2022; Liang 2013; Liu and Pu 2019; Jiang et al. 2019; Komatsu et al. 2023; Vannitsem and Liang 2022). More recently, Komatsu et al. (2023) applied the Liang–Kleeman information flow analysis for examining the causal relation between snow cover fraction (SC) and SAT over the autumnal Eurasian continent and successfully delineated the SC–SAT causality on a sub-monthly timescale. By extending the work of Komatsu et al. (2023), this study aims to identify "cold spots" (Xu and Dirmeyer 2013), where the SC condition actively controls SAT time-evolution on a sub-monthly timescale, and compare the snow impacts among models. This study analyses the SC–SAT interaction in the Northern Hemisphere from September to May to provide its holistic view. Furthermore, we evaluate the SC–SAT causal relation in sub-seasonal prediction

models using reforecast data provided by the WWRP/WCRP S2S Project (Vitart et al. 2017).

The rest of this paper is organised as follows. Section 2 describes the data used in this study and the Liang–Kleeman information flow analysis. In Sect. 3, observed sub-monthly causal relations between SC and SAT are examined using reanalysis data. In addition, the S2S prediction models are evaluated in terms of the SC–SAT causality. Possible reasons for the identified deficiency of the JMA model are also discussed. Moreover, the association between snow causality and SAT predictability are examined to evaluate potential contributions of snow conditions to enhancing SAT prediction skill. Section 4 gives conclusions and discussion.

2 Data and methods

2.1 Data

We used daily SC, SWE, and SAT data from the National Aeronautics and Space Administration (NASA) Modern-Era Retrospective analysis for Research and Applications, Version 2 (MERRA-2) reanalysis during 2000–2020 (Gelaro et al. 2017). MERRA-2 reanalysis uses the model of the NASA Global Modeling and Assimilation Office (GMAO) GEOS-5.12.4 system with an approximate resolution of $0.5° \times 0.625°$. The land surface model of MERRA-2 is the Catchment model (Koster et al. 2000; Reichle et al. 2011). Time-evolution of SWE, snow depth, and snow heat content are solved using a three-layer snow model (Stieglitz et al. 2001). In the MERRA-2 system, no snow observational data is assimilated, however, model-based precipitation is corrected using gauge- and satellite-based precipitation observations (Reichle et al. 2017). The MERRA-2 land analysis is in reasonably good agreement with other in-situ and satellite-based observations (Reichle et al. 2017) and has the comparable performance with other reanalysis and satellite-derived products (Mortimer et al. 2020). We present results based on ERA5 (Hersbach et al. 2020) as well as MERRA-2 data.

As for S2S prediction data, we used reforecast data obtained from the data archive of the WWRP/WCRP S2S Prediction Project hosted by the European Centre for Medium-Range Weather Forecasts (ECMWF; Vitart et al. 2017). We analysed reforecast data of three operational centres that provide SC data: China Meteorological Administration (CMA, BCC-CPS-S2Sv2), ECMWF (CY47R1), and Japan Meteorological Agency (JMA; GEPS2203). The BCC-CPS-S2Sv2, CY47R1, and GEPS2203 adopt land schemes of Beijing Climate Center Atmospheric Vegetation Interactive Model version 2 (BCC-AVIM2; Li et al. 2019), the Hydrology-Tiled ECMWF Scheme for Surface Exchanges over Land (HTESSEL; Balsamo et al. 2009; Dutra et al. 2010), and the Simple Biosphere (SiB) scheme (Hirai et al. 2007; Japan Meteorological Agency 2023), respectively. Specifications of the reforecasts analysed in this study are summarised in Table 1. Note that we analysed reforecasts with the same ensemble size of 11 members for the ECMWF and JMA models, and 4 members for the CMA model due to data availability. Since initial dates of reforecasts are not common among the models, we chose the reforecasts with initial dates nearest to the first day of the month. All the observational and model data were interpolated to regular $2.5° \times 2.5°$ latitude–longitude grids using bilinear interpolation, and then the daily climatology of the analysed period was subtracted prior to the Liang–Kleeman information flow analysis.

2.2 Liang–Kleeman information flow analysis

Conventional statistical analyses using Pearson correlation coefficient or linear regression, which are widely used in climate research, can detect linear association between two variables. These statistical analysis techniques have been extensively used for evaluating the strength of the land–atmosphere interaction (e.g., Dirmeyer 2011; Dirmeyer et al. 2014; Ganeshi et al. 2023; Xu and Dirmeyer 2013). However, these techniques cannot directly infer the causal direction. A lag correlation is also often used to investigate the causality in the climate system. It is, however, prone to misdetection of the causality due to the long memory (autocorrelation) of variables (McGraw and Bernes 2018).

An alternative and novel technique to quantify the causality is Liang–Kleeman information flow. Here, we briefly describe the Liang–Kleeman information flow analysis used in this study. Liang and Kleeman (2005) derived a rigorous formulation to evaluate the causality (information transfer) in a two-dimensional dynamical system. Consider a two-dimensional stochastic system,

$$d\boldsymbol{X} = \boldsymbol{F}(\boldsymbol{X}, t)dt + \boldsymbol{B}(\boldsymbol{X}, t)d\boldsymbol{w}, \tag{1}$$

where $\boldsymbol{F} = \left(F_1, F_2\right)^T$ and $\boldsymbol{B} = \begin{pmatrix} b_{11} & b_{12} \\ b_{21} & b_{22} \end{pmatrix}$ are functions of $\boldsymbol{X} = \left(x_1, x_2\right)^T$ and t, and $\boldsymbol{w} = \left(w_1, w_2\right)^T$ is a two-dimensional Wiener process (white noise), and the superscript of T represents the transpose operation. Liang (2008) derived the rate of information flow from x_2 to x_1 as

$$T_{2\to1} = -E\left[\frac{1}{\rho_1}\frac{\partial\left(F_1\rho_1\right)}{\partial x_1}\right] + \frac{1}{2}E\left[\frac{1}{\rho_1}\frac{\partial^2\left(b_{11}^2 + b_{12}^2\right)\rho_1}{\partial x_1^2}\right], \tag{2}$$

Table 1 Specification of reforecast data analysed in this study

Centre	Model version	Initial month/initial date (reforecast period)	Ensemble size
CMA	BCC-CPS-S2Sv2	September/3 September (2005–2019) October/1 October (2005–2019) November/2 November (2005–2019) December/3 December (2005–2019) January/4 January (2006–2020) February/1 February (2006–2020) March/1 March (2006–2020) April/1 April (2006–2020) May/3 May (2006–2020)	4
ECMWF	CY47R1	September/3 September (2000–2019) October/10 October (2000–2019) November/2 November (2000–2019) December/3 December (2000–2019) January/4 January (2001–2020) February/1 February (2001–2020) March/1 March (2001–2020) April/1 April (2001–2020) May/3 May (2001–2020)	11
JMA	GEPS2203	September/31 August (2000–2019) October/30 September (2000–2019) November/31 October (2000–2019) December/30 November (2000–2019) January/31 December (2000–2019) February/31 January (2001–2020) March/28 February (2001–2020) April/31 March (2001–2020) May/30 April (2001–2020)	11

where E stands for expectation, ρ_1 is the marginal probability density of x_1. This expression is rigorous, however, computing the information flow in real-world problems requires a prior knowledge of the Eq. (1), which is usually unknown. Instead, Liang (2014) derived a formula of approximate information flow by fitting $\boldsymbol{F}$ with a linear stochastic function of $\boldsymbol{X}$ obeying the Gaussian distribution. The Liang–Kleeman information flow ($T_{2\to1}$), which is an approximate transfer entropy indicating the information transfer from X_2 to X_1, is written as.

$$T_{2\to1} = \frac{C_{11}C_{12}C_{2,d1} - C_{12}^2 C_{1,d1}}{C_{11}^2 C_{22} - C_{11}C_{12}^2}, \tag{3}$$

where C_{ij} is the sample covariance between X_i and X_j, and $C_{i,dj}$ is the sample covariance between X_i and the time derivative of X_j using the Euler forward scheme (Liang 2014). Following Liang (2015), we present the normalised information flow in this paper (hereafter simply referred to as causality) as in Komatsu et al. (2023). The proofs and complete derivation of the formula are referred to Liang and Kleeman (2005), Liang (2008, 2014, 2015).

3 Results

3.1 Climatological features of SC

This subsection describes the climatological features of SC in the Northern Hemisphere. Figure 1 shows the standard deviation of weekly (7-day) mean SC by month. Intuitively, regions with large SC variability are expected to have a potentially strong influence on SAT variability in the first place (Xu and Dirmeyer 2013). Regions with large SC variance migrate seasonally between Northern Siberia and Alaska in September to the midlatitudes over Eurasia and North America in February, then move northward into late spring. The regions with large SC variability roughly coincide with transition regions with climatological mean SC of about 50% (black lines in Fig. 1), indicating large SC variability regions appear in the SC transition regions. Conversely, regions and seasons with high climatological mean of SC (e.g., Arctic regions in boreal winter) have small subseasonal variability because SC is always close and equal to 100%.

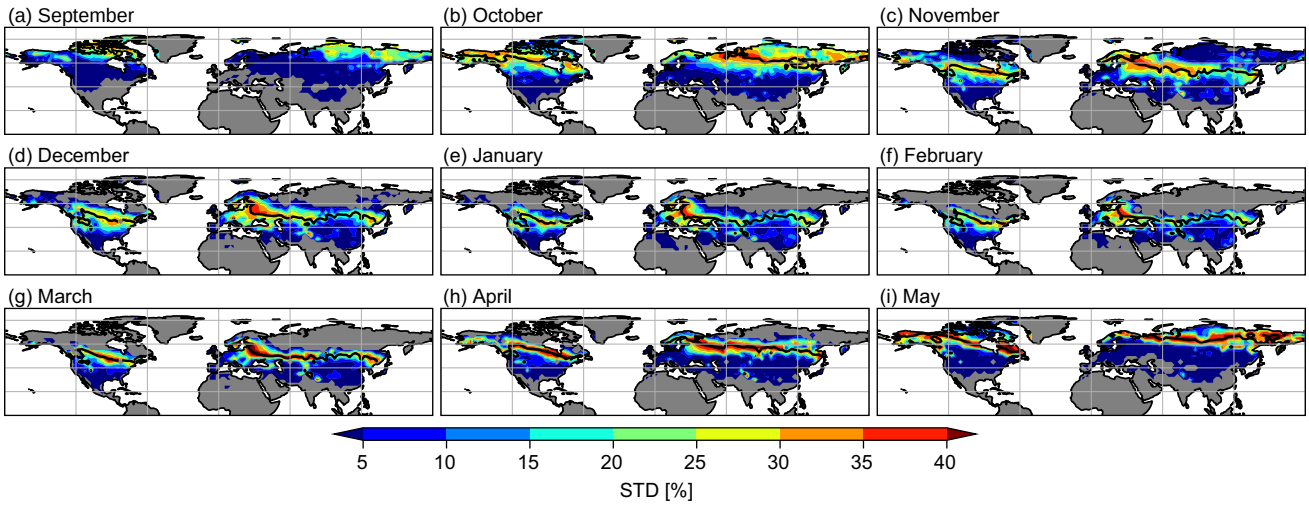

Fig. 1 Seasonal migration of large SC variability regions. Colours show the standard deviation of weekly average SC [%] of MERRA-2 reanalysis for each month. MERRA-2 SC data of four consecutive weeks starting from 1st of the month (denoted in each panel) during (a-d) 2000–2019 (e-i) 2001–2020 were used. Black lines indicate climatological mean SC of 50%

Figure 2a displays simultaneous Pearson correlations between weekly averages of SAT and SC from the MERRA-2 reanalysis data. We found negative correlations in the large SC variability regions and seasons (Fig. 1), indicating SAT tends to be low when SC is high and vice versa. It may be intuitive that low SAT co-occurs with more SC over the SC marginal regions, however, this correlation does not necessarily indicate causality, and we cannot infer which causes which based on the correlation analysis. Similarly, Fig. 2b shows correlations between weekly averages of SAT and SWE. The negative correlation regions roughly coincide with the results for SC. Meanwhile, it is noteworthy that weak positive correlation regions spread over the northern Eurasia in boreal winter consistent with the result of the study by Diro and Lin (2020), indicating SWE tends to be high when SAT is high and vice versa. This is plausibly due to increased snowfall associated with the fact that more moisture is retained at a higher temperature but below freezing point of water (Clausius–Clapeyron relationship; Davis et al. 1999). In the next subsection, the distinct relationship between snow and SAT is further illustrated using the causality analysis in more detail.

3.2 Observed sub-monthly causal relations between SC and SAT

We investigate the observed causal relationship between SC and SAT using the Liang–Kleeman information flow analysis. Figure 3 displays normalised information flow between weekly averages of SC and SAT by month. In observations (MERRA-2 reanalysis), the cold spots, which refer to strong causality regions from SC to SAT, are stipulated by geographical location and season. We determine the cold spots based on a criterion that a region with normalized causality exceeding 5% covers a relatively large area ($> 4 \times 10^6 \mathrm{km}^2$). The cold spots are found around North Eurasia in September and October; East Siberia in October and May; Canada in November; East Asia in November and March; Central Asia in October and November; and Eastern Europe in March. This result indicates that cold spots of SC-SAT interactions change their location during different months and are mostly located around the regions where SC variability is larger (Figs. 1 and 3). We note that regions with surface air temperature of the melting point (climatological mean temperature of 0 °C) do not always coincide with the significant cold spots (Figs. 3 and S1). We observe a stronger coincidence between the cold spots and regions with the large SC variability regions than regions at the melting point of surface air temperature (climatological mean temperature of 0 °C; Fig. S1), presumably due to the primary influence of the snow-albedo effect rather than the snow hydrological effect on sub-monthly timescales.

In addition, we evaluated information flow between SWE and SAT using the MERRA-2 data (Fig. S2). Regions with the high causality from SWE to SAT generally match the cold spots for SC. In contrast, the opposite causality from SAT to SWE spreads over broader regions and its amplitude is stronger, compared with the SC counterparts. These differences are due to the fact that the SC reaches an upper limit of 100% when SWE exceeds a certain level. As seen in Figs. 2, 3 and S2, simple simultaneous correlation analysis between SAT and SC or SWE may falsely detect the cold spots (regions with actual snow effect). Therefore, we

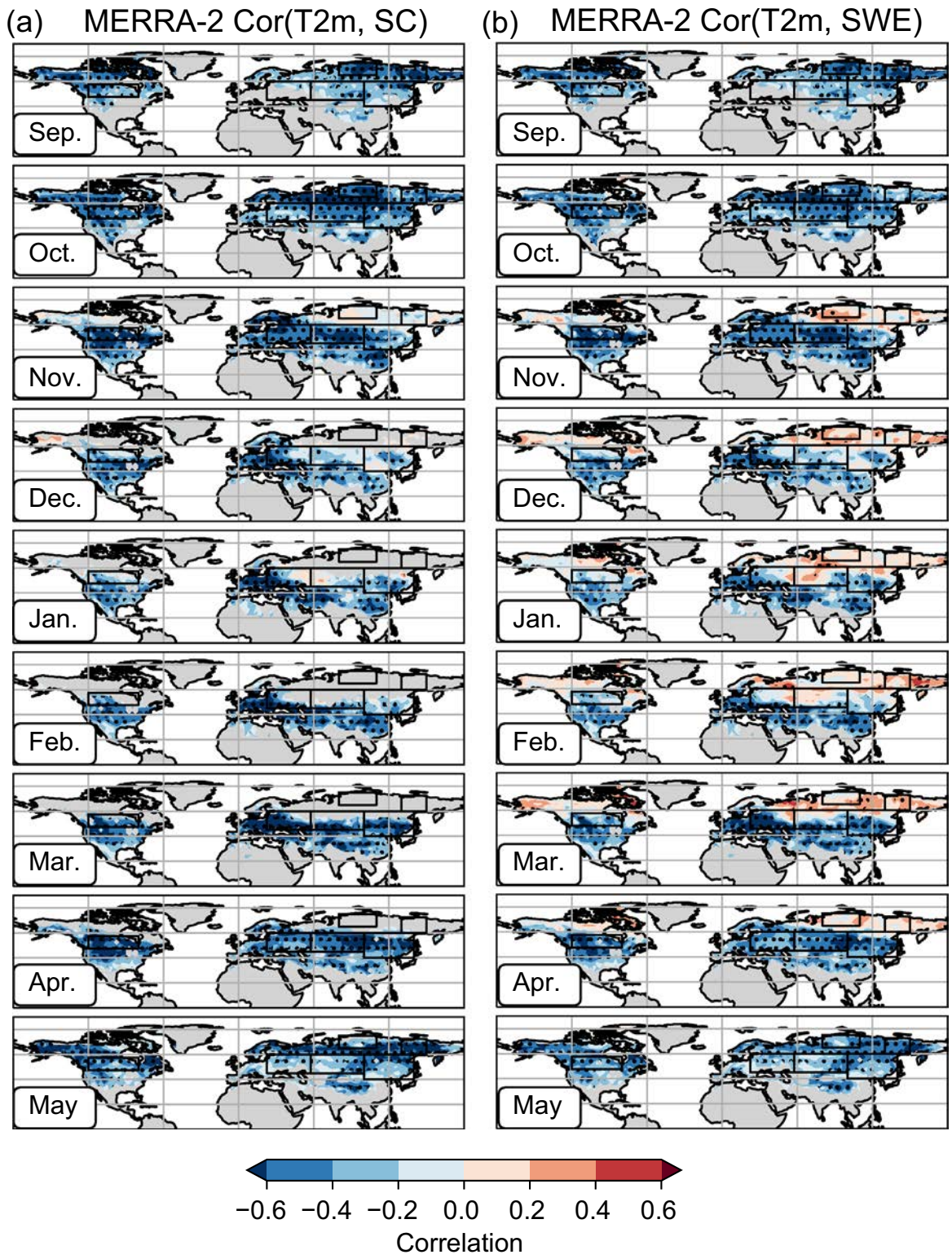

Fig. 2 Correlations between weekly averages of SAT and (**a**) SC, (**b**) SWE in MERRA-2 analysis. Areas where the snow covers the ground for more than one third of the period are coloured. Analysed years for each month are the same as the reforecast periods of the ECMWF and JMA models shown in Table 1. The stippling indicates statistically significant regions based on the bootstrap method (5,000 times resampling). Boxes indicate cold spots identified in this study (Sect. 3.2)

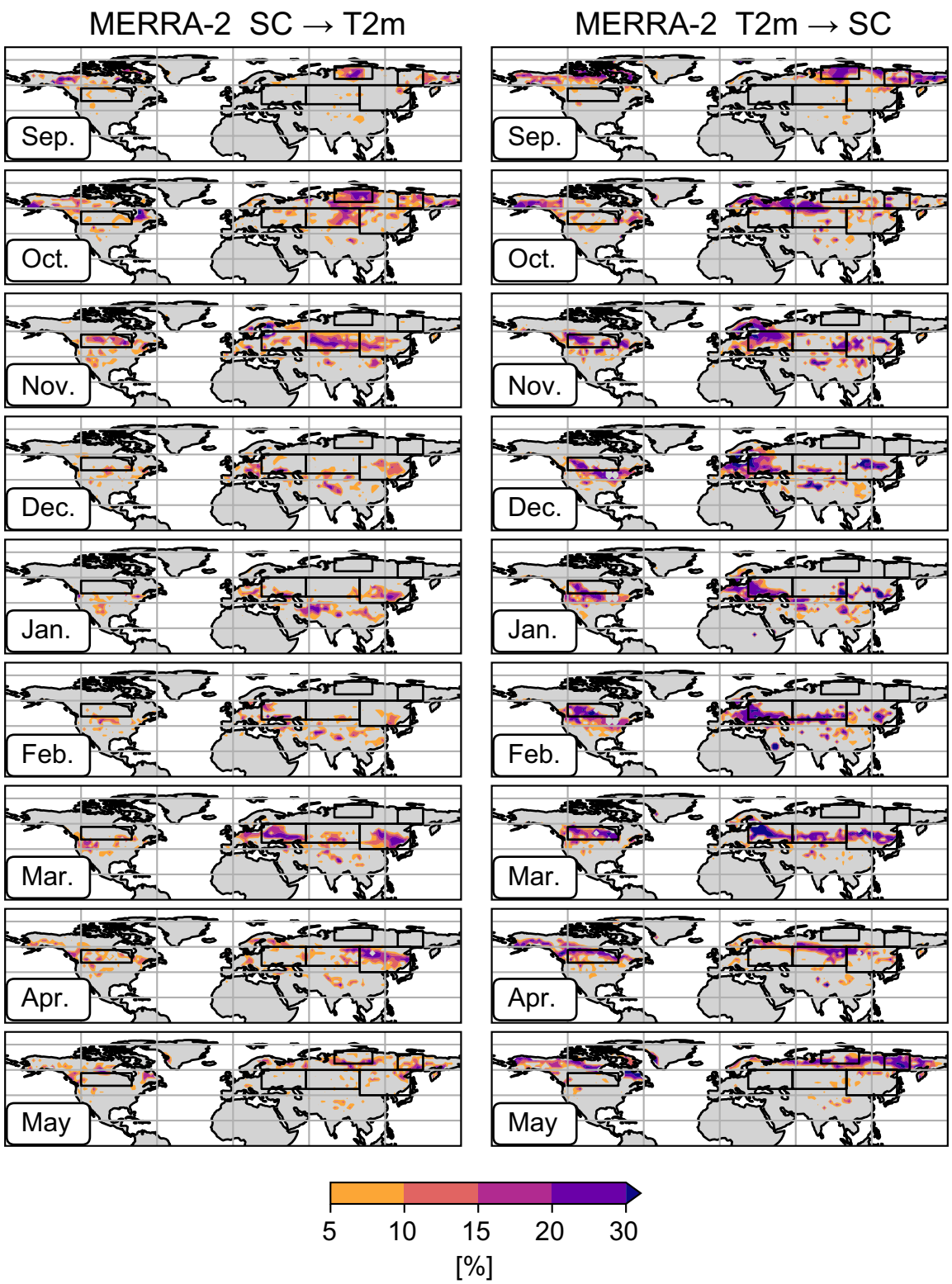

Fig. 3 Normalised information flow between weekly averages of SC and SAT by month. The normalised information flow (right) from SC to SAT, and (left) from SAT to SC. The MERRA-2 reanalysis data of four consecutive weeks (7 days averages) starting from 1st of the month (denoted in each panel) were used for the calculation for each month. Boxes indicate cold spots identified in this study: East Siberia (60°N–72.5°N, 130°E–150°E), East Asia (40°N–60°N, 100°E–140°E), Canada (47.5°N–57.5°N, 120°W–80°W), Eastern Europe (45°N–60°N, 22.5°E–57.5°E), Central Asia (45°N–60°N, 57.5°E–100°E), North Eurasia (65°N–75°N, 80°E–110°E). Only statistically significant regions based on the bootstrap method (5,000 times resampling) are coloured

consider that the information flow analysis based on SC is advantageous to examine the snow–atmosphere interaction and to determine the cold spots.

We also examined the information flow in ERA5 reanalysis (Fig. S3) and found that overall spatial distributions are similar to the results of the MERRA-2 reanalysis shown here. Therefore, we consider that the overall results presented here are not so sensitive to the dataset used, with noting that the strength of the causality more or less changes. Specifically, in the ERA5 reanalysis, there are stronger cold spots in high terrain regions such as the Tibetan Plateau than MERRA-2, presumably due to an excessive land snow in ERA5 (Orsolini et al. 2019). Also, weaker cold spots are seen over North America in the ERA5 reanalysis than in the MERRA-2 reanalysis. The difference may arise from the uncertainty of both reanalysis products, thus the results over such regions should be interpreted with caution because of relatively large uncertainty in reanalysis data.

Figure 4 illustrates the seasonality of the SC–SAT causality for the cold spots identified in Fig. 3. A distinct seasonality is found for each cold spot. The high-latitude cold spots, East Siberia (60°N–72.5°N, 130°E–150°E) and North Eurasia (65°N–75°N, 80°E–110°E) have profound double peaks of the information flow from SC to SAT in autumn (September and October) and late spring (May). The northern mid-latitude cold spots, Canada (47.5°N–57.5°N, 120°W–80°W), Eastern Europe (45°N–60°N, 30°E–60°E), and Central Asia (45°N–60°N, 57.5°E–100°E) have also double peaks of the causality from SC to SAT with the stronger causality in winter. In the mid-latitude cold spot, East Asia (40°N–60°N, 100°E–140°E) has a prolonged period of the causality from SC to SAT from November to April with the stronger causality from SC to SAT in spring. Previous studies suggested that the snow influence on SAT is stronger in spring than the other seasons because of stronger snow–albedo and snow hydrological effects during a snow melting season (Xu and Dirmeyer 2013; Zhang et al. 2005). Meanwhile, there are some regions, for example, East Asia and Canada, that have sizable causality from SC to SAT in autumn. The high causality from SC to SAT over East Asia in November was highlighted by Komatsu et al. (2023). As presented here, the snow causality varies significantly by month. Our results highlight stark contrast in the snow effect on SAT among months (Figs. 3 and 4).

It is emphasised that more often than not, the causality from SC to SAT accompanies the opposite causality (from SAT to SC). The normalised causality is overall larger from SAT to SC than from SC to SAT. This result suggests that over the cold spots, positive feedback works between SC and SAT, amplifying the SC–SAT interaction. We also note that the causality from SWE to SAT presents similar seasonality

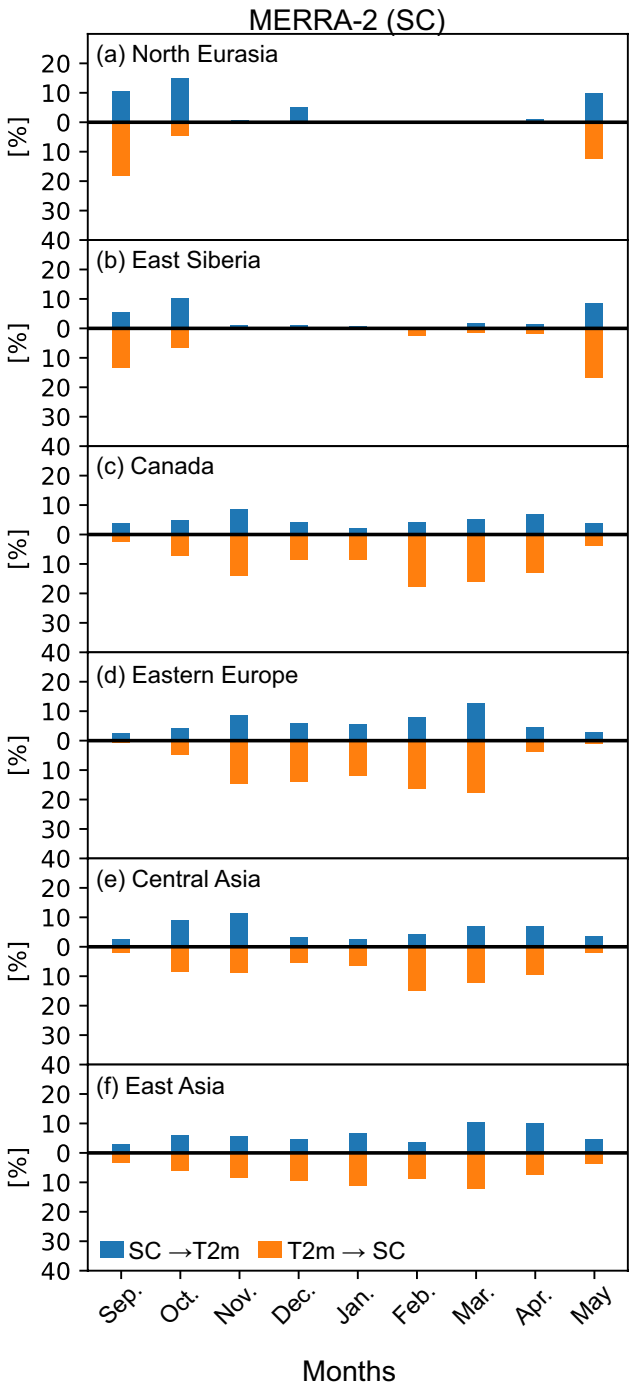

Fig. 4 The seasonality of the SC–SAT causality averaged over the cold spot regions (land only). Blue bars indicate the normalised causality from weekly mean SC to weekly mean SAT. Orange bars indicate the normalised causality from weekly mean SAT to weekly mean SC. Regions are denoted in the figure: North Eurasia (65°N–75°N, 80°E–110°E), East Siberia (60°N–72.5°N, 130°E–150°E), Canada (47.5°N–57.5°N,120°W–80°W), Eastern Europe (45°N–60°N, 30°E–60°E), Central Asia (45°N–60°N, 57.5°E–100°E), and East Asia (40°N–60°N, 100°E–140°E)

with the counterpart of SC, except that the causality from SAT to SWE appears through winter over North Eurasia and East Siberia unlike the causality from SAT to SC (Fig. S4).

3.3 Evaluation of S2S prediction models

Next, we attempt to evaluate the SC–SAT causal relation in operational S2S models. Information flow (Liang 2014) is a fundamental quality to measure the causality, and thus, can be potentially used to evaluate the fidelity of models in representing the snow-atmosphere interaction (e.g., the strength of the interaction). Figures 5, 6, and 7 present the SC–SAT causality in the S2S models. The causality is computed using predictions of four consecutive weeks (Week 1-Week 4). The models generally capture the observed pattern and seasonality of the causality except for the JMA model with the rather weak causality from SC to SAT, although there are some notable discrepancies between the models and reanalysis.

As for the ECMWF model (Figs. 5 and 8; Table 2), the pattern and amplitude are generally in good agreement with those of the MERRA-2 reanalysis with the weaker causality from SC to SAT over Eastern Europe in March, East Asia in March and April, and North Eurasia in September and October, and the stronger causality over the Tibetan Plateau.

The JMA model (Figs. 6 and 8; Table 2) considerably underestimates the causality for both directions, in particular from SC to SAT. This result indicates that SAT does not realistically respond to SC conditions, and SC does not respond well to SAT either. Although SC is a diagnostic variable, we also obtained consistent results for causality based on SWE, which is a prognostic variable (Fig. S6). Based on these results, we conclude that the JMA model underestimates the snow effect on SAT on a sub-seasonal timescale. Possible reasons for the underestimation of causality will be discussed later.

As for the CMA model (Figs. 7 and 8; Table 2), the causality pattern is overall in good agreement with that of the MERRA-2 reanalysis with the underestimated amplitude compared to the MERRA-2 reanalysis. The causality from SC to SAT over North Eurasia in September, and October is underestimated. Over the Tibetan Plateau, the causality is stronger than the MERRA-2 reanalysis in winter.

Overall, the S2S models analysed in this study tend to underestimate the snow influence on SAT except for over the Tibetan Plateau. The conclusions do not change much when we use the ERA5 reanalysis as reference data, however, there is uncertainty among the reanalysis, models, and in-situ observation, particularly in high terrain regions such as the Tibetan Plateau (Orsolini et al. 2019). We also note that the results for Weeks 1–2 tend to exhibit greater values, which can be attributed to the impact of initialization, as well as the initial shocks and drifts experienced during the first two weeks. Conversely, the results for Weeks 3–4 align more closely with the results for Weeks 1–4 presented here. It is noted that the characteristics described here are also valid for the evaluation based on SWE (Figs. S5, S6, and S7; Table 2), and therefore, the results presented here provide an evaluation of a proxy of the snow influence strength. The results uncover the capability of representing the snow influence in the current S2S models.

3.4 Reasons for the weak causality in the JMA model

We found that the JMA model particularly underrepresents the snow influence on SAT. Here we briefly discuss possible reasons for this deficiency. The snow influence in a model may be related to its climatology of variability and mean of SC. Figure 9 compares the standard deviations of weekly mean SC of reforecasts for the (left) ECMWF and (middle) JMA models for each month. The large SC variability regions in the JMA model locate southward compared to the ECMWF model (Fig. 1).

We also verified the mean SC biases of the ECMWF and JMA models (Fig. 10). The mean bias in the ECMWF is much smaller than that in the JMA model, which has excessive SC around the SC transition regions. The southward shift of the large SC variability regions in the JMA model may be attributable to the excessive SC. The excessive SC bias was also found in the verification against the MODIS/Terra snow cover data (Hall and Riggs 2021; not shown). The SC bias in the JMA model may be associated with the underestimation of SC variability and SC influence on SAT. The modelled SC depends on the SC diagnostics equation (parameterisation; Yonehara et al. 2020) and is used in the land surface processes (e.g., albedo, heat fluxes). The biased SC climatology may be a primary reason for the underestimation of the causality from SC to SAT. In short, the verification results of the model climatology imply that the SC biases in mean and variance may account for the underestimated causality in the JMA model. However, the SC-SAT interaction is affected by not only the land processes, but also atmospheric processes such as atmospheric boundary layer, radiation, and cloud processes, thus, we need more detailed analysis using model sensitivity experiments to underpin this point.

3.5 Influence on SAT predictability

In Sects. 3.2 and 3.3, we investigated the observed and simulated causality between snow and SAT. Now a question arises: To what extent does the snow condition affect prediction skill and predictability in S2S prediction? Answering this question from reforecasts of multiple models is not straightforward since the prediction skill in different models

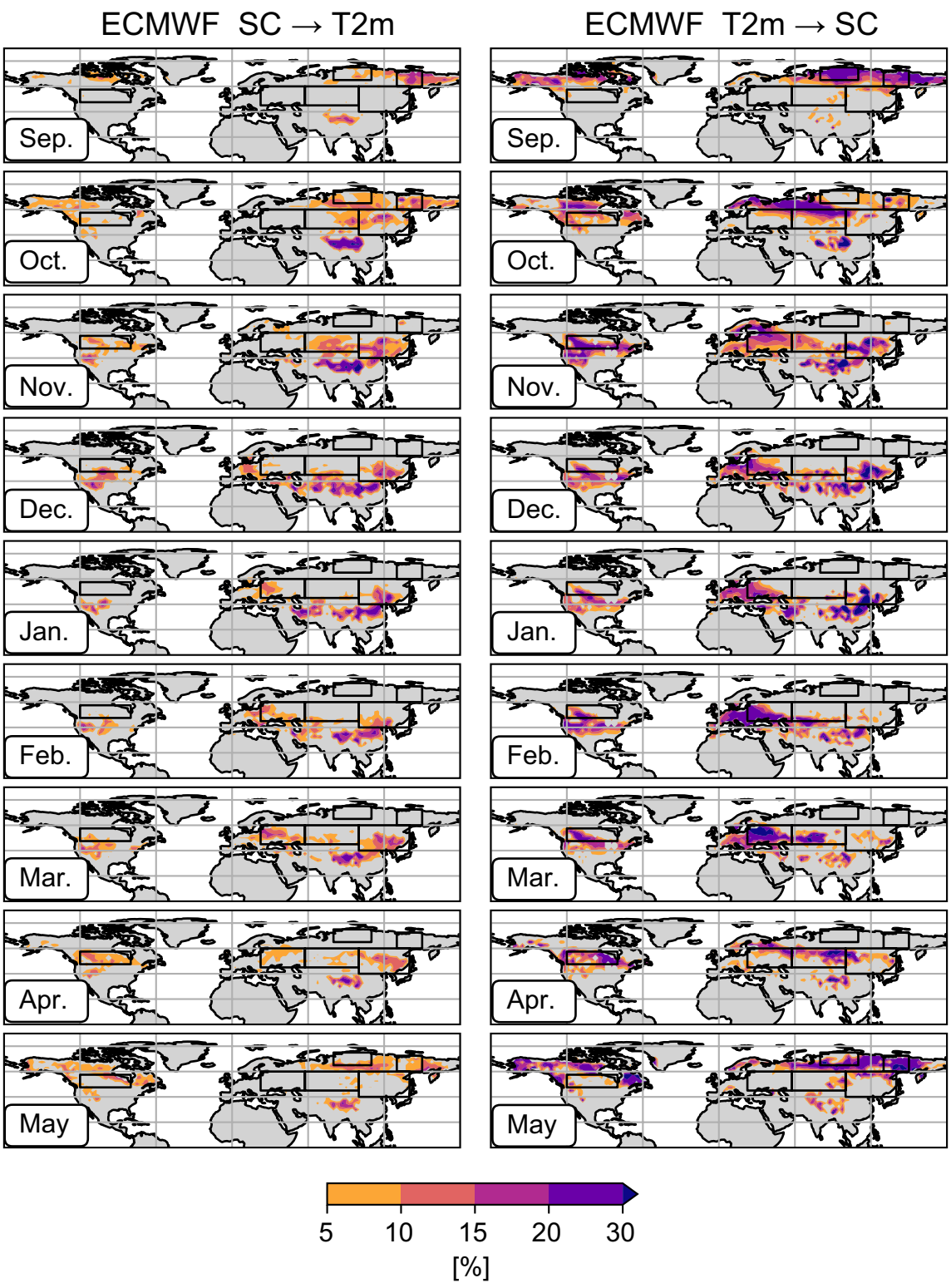

Fig. 5 Same as Fig. 3 but for the ECMWF model

depends on the prediction performance of many factors other than snow conditions. Thus, it is difficult to delineate the contribution of snow on the SAT prediction skill. Instead, we examine the potential predictability of SAT in the ECMWF and JMA models to address the potential contribution of SC on sub-seasonal SAT predictability. The potential

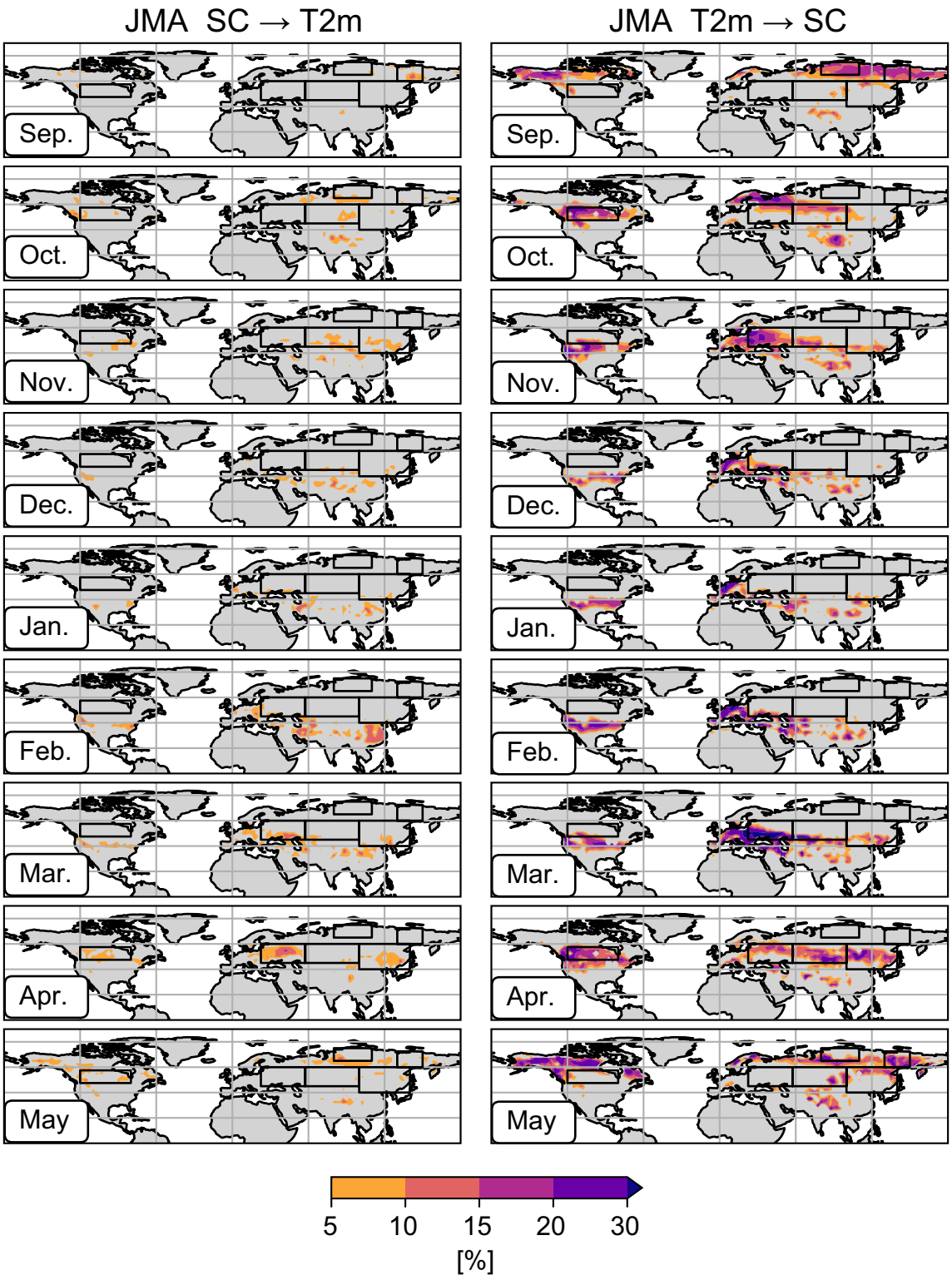

Fig. 6 Same as Fig. 3 but for the JMA model

predictability was assessed using ensemble predictions under the perfect model assumption. Specifically, we have computed the potential predictability assessed by squared Pearson correlation between a randomly selected member as a surrogate observation against an ensemble mean prediction of the rest of the ensemble members (Takaya et al. 2021).

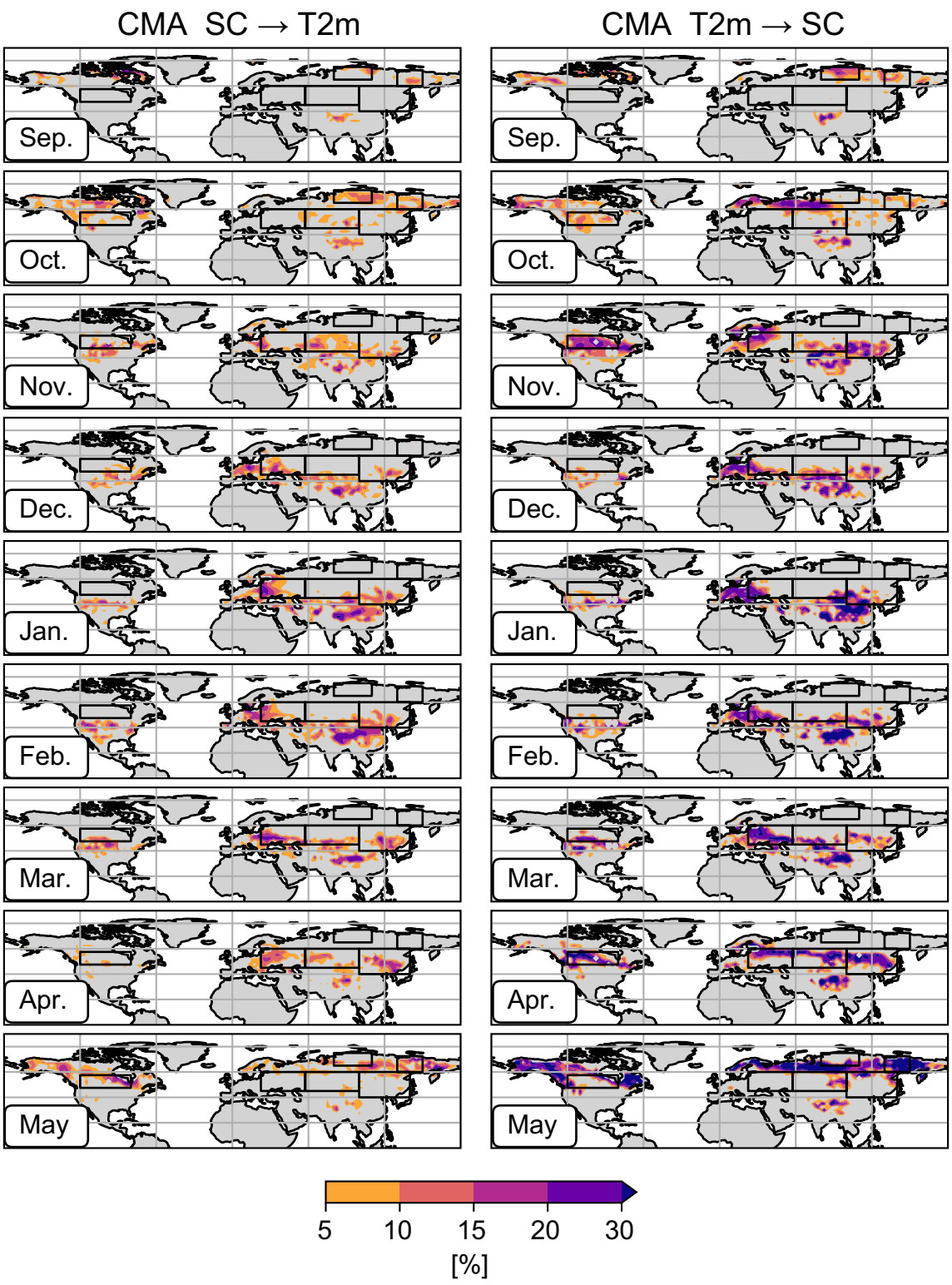

Fig. 7 Same as Fig. 3 but for the CMA model

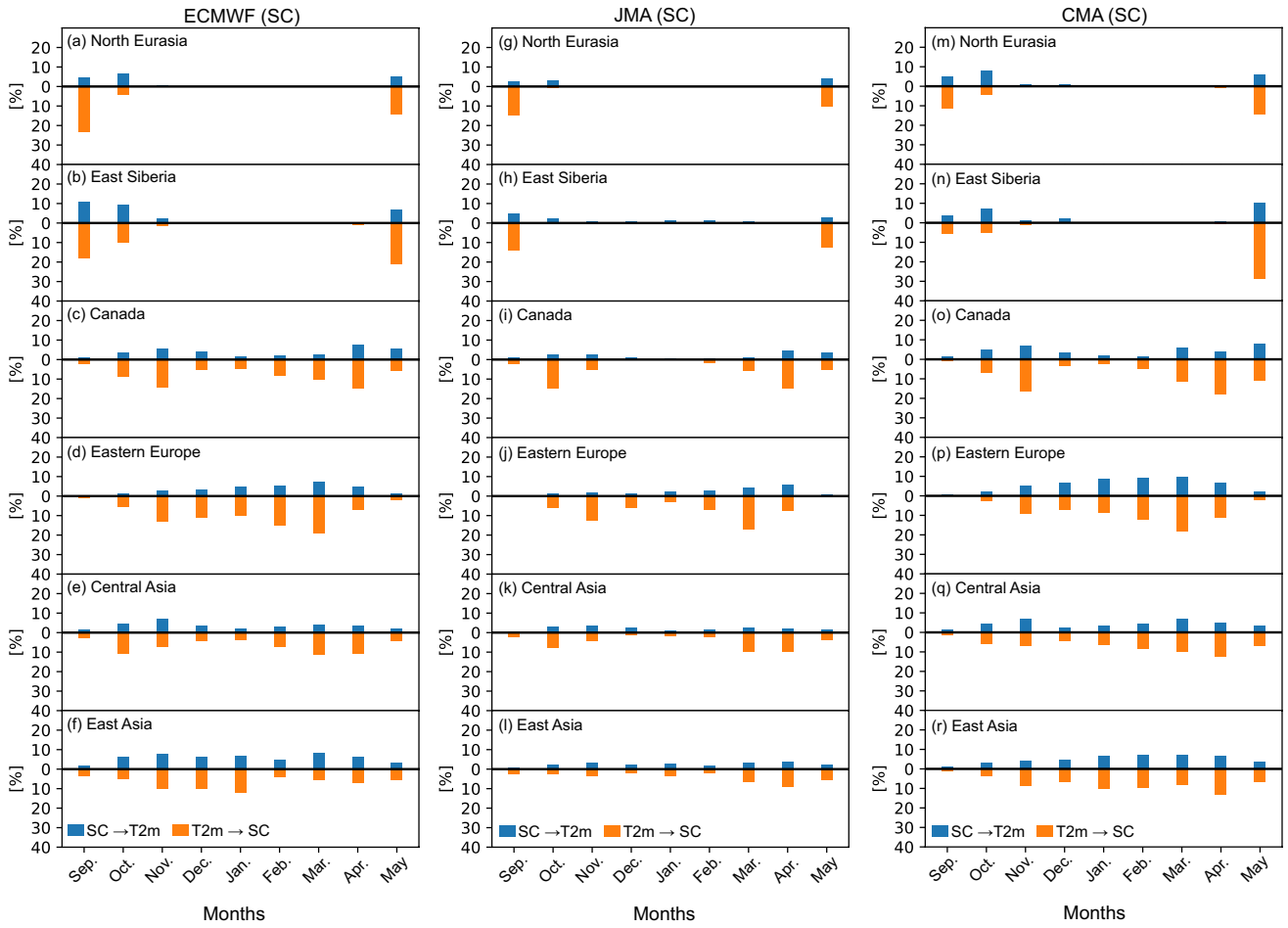

Fig. 8 Same as Fig. 4 but for the S2S models (left: ECMWF model, middle: JMA model, right: CMA model)

Table 2 Summary of the causality (the normalised causality from weekly mean SC and SWE to weekly mean SAT [%]) in the identified cold spots

Region (month)	Normalised causality (SC→T2m) Reanalysis/S2S model					Normalised causality (SWE → T2m) Reanalysis/S2S model				
	MERRA-2	ERA5	ECMWF	JMA	CMA	MERRA-2	ERA5	ECMWF	JMA	CMA
North Eurasia (October)	15	10	7	2	8	8	9	7	2	2
East Siberia (October)	10	7	9	1	7	6	6	6	5	2
Canada (November)	9	8	6	1	6	7	4	3	1	2
Eastern Europe (November)	12	8	6	2	7	11	10	5	4	2
Central Asia (March)	12	8	6	2	7	11	10	5	4	2
East Asia (March)	10	8	7	1	5	6	3	2	2	2

This procedure was repeated 5,000 times, and averages of the results are presented.

Figure 11 displays the potential predictability for two-week averages of SAT at a lead time of one week (prediction for Weeks 2 and 3). The potential predictability over the cold spots tends to be lower in the JMA model than in the ECMWF model (Figs. 11). This reflects, at least partly, the fact that the causality from snow to SAT is lower in the JMA model than in the ECMWF model, implying the importance of faithfully representing the SC effect in models for further improving the sub-seasonal forecast skill.

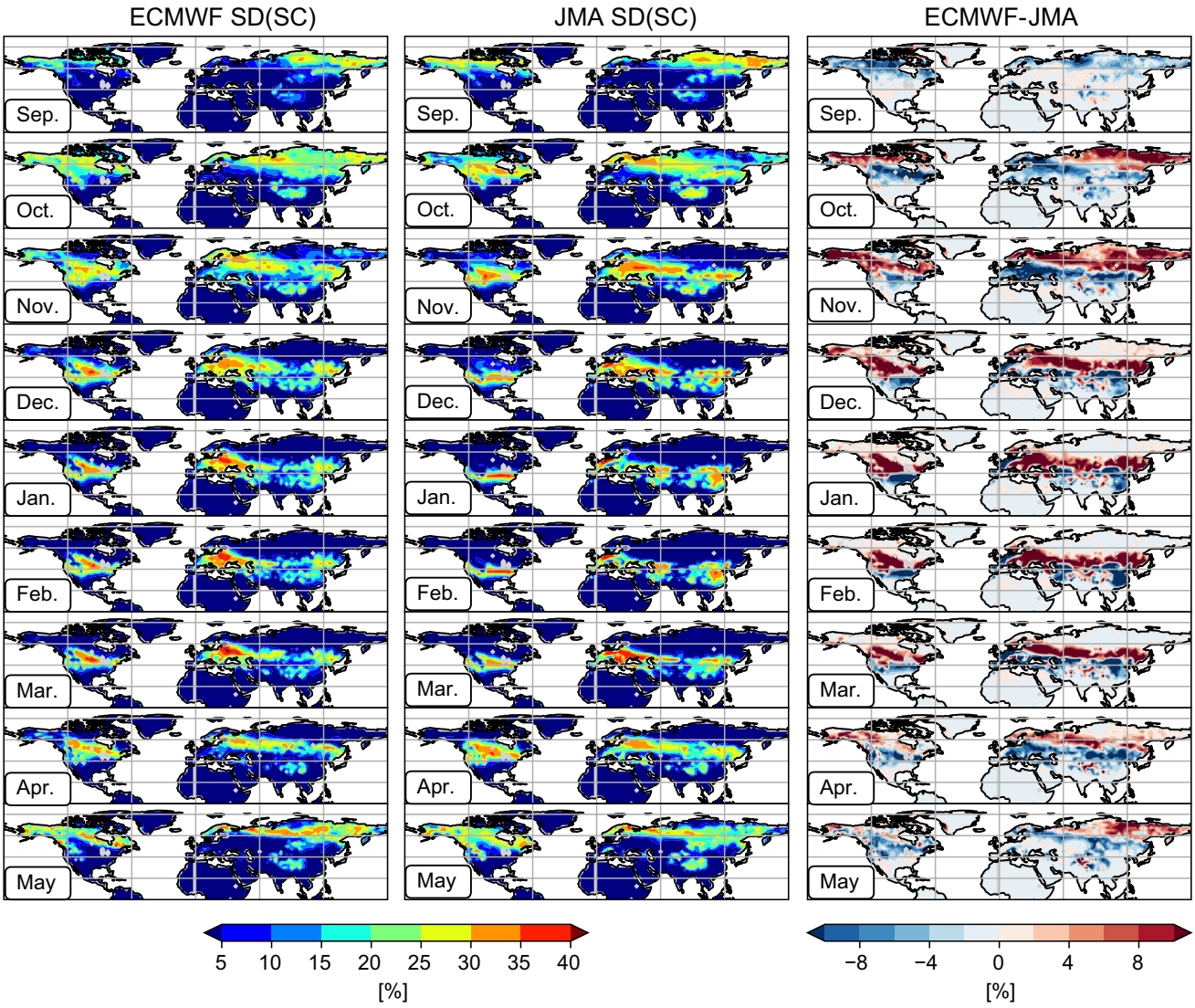

Fig. 9 Standard deviations of weekly-mean SC in reforecasts of (left) ECMWF and (middle) JMA models for each initial. (Left) Differences between the ECMWF and JMA models. Initial months are denoted in the bottom left of each figure

4 Summary and discussion

In this study, we used a novel analysis technique, Liang–Kleeman information flow, to investigate the causality between snow cover and surface temperature variability on a sub-monthly timescale. The causality in the snow–SAT interaction was successfully described using the analysis technique. Although the information flow analysis does not always provide conclusive results, we demonstrated its usability for diagnosing the strength and direction of causation (cause and effect relationship) in the snow–SAT interaction on a sub-monthly timescale. Based on the results, we identified cold spots, which refer to regions where land snow exerts a significant influence on SAT. The cold spots are stipulated by geographical location and season, and are identified over North Eurasia in September and October; East Siberia in October and May; Canada in November; East Asia in November and March, Central Asia in October and November, and Eastern Europe in March. Figure 12 summarises the cold spots identified in this analysis. These cold spots are also supported by the same analysis for SWE instead of SC.

The identified cold spots in this study generally match the snow-sensitive regions that previous studies obtained based on the change of the SAT potential predictability in a set of sensitivity experiments by changing snow initial conditions. Jeong et al. (2013) found that the SAT predictability is increased by realistically initialising snow conditions over central and eastern parts of the Eurasian continent in November–April, northwestern parts of the United States

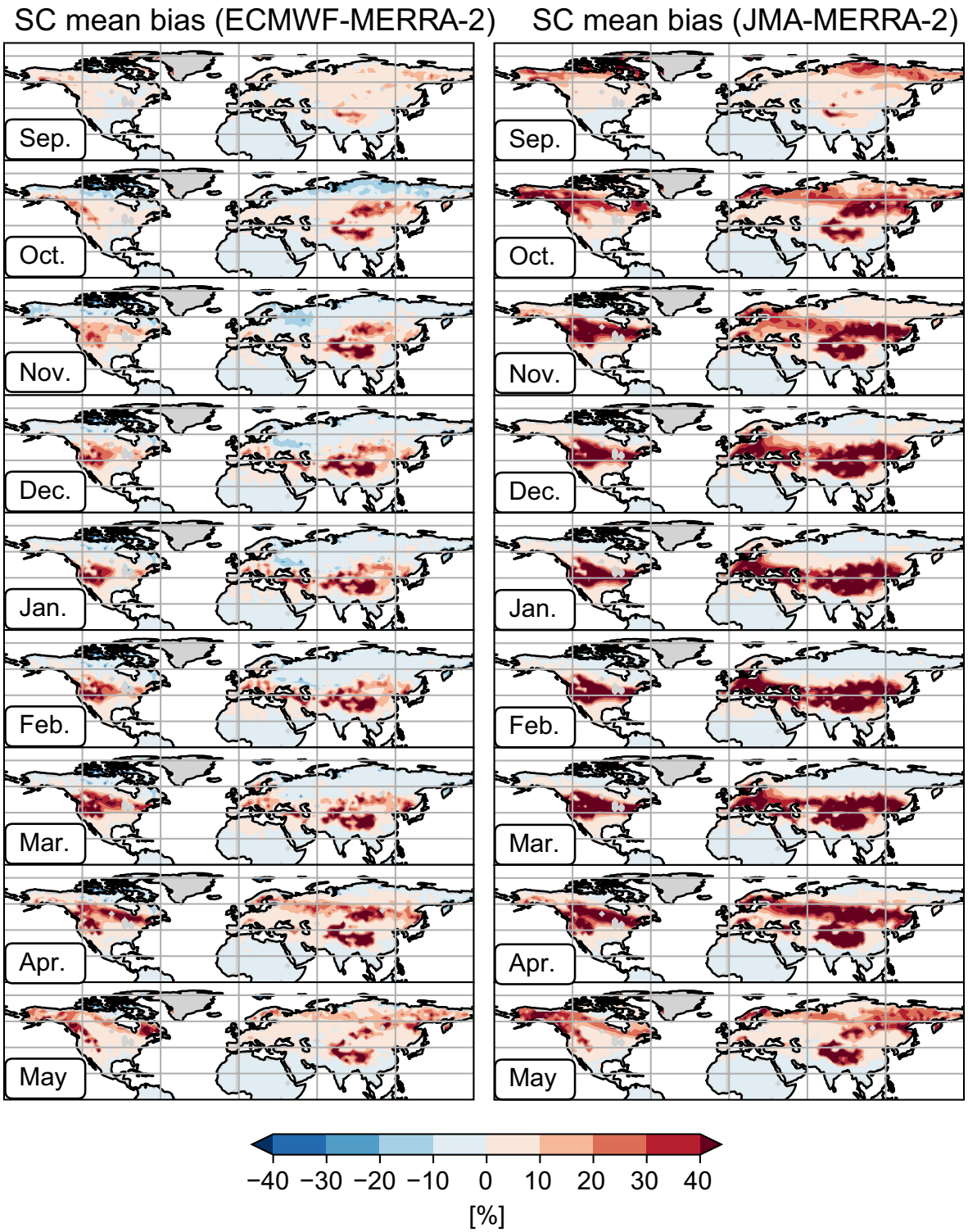

Fig. 10 Mean biases of weekly-mean SC in reforecasts of the (left) ECMWF and (middle) JMA models against MERRA-2 reanalysis for each initial. Initial months are denoted in the bottom left of each figure

in January–April, and the Tibetan Plateau in the whole cold season (September–April). The cold spots of this study are generally contained in the regions identified by Jeong et al. (2013). It is noteworthy that the cold spots identified in this study are more confined in terms of location and timing than the previous study (Fig. 4 of Jeong et al. 2013) because we considered a month-to-month change in the snow conditions. The advantages of the Liang–Kleeman information flow

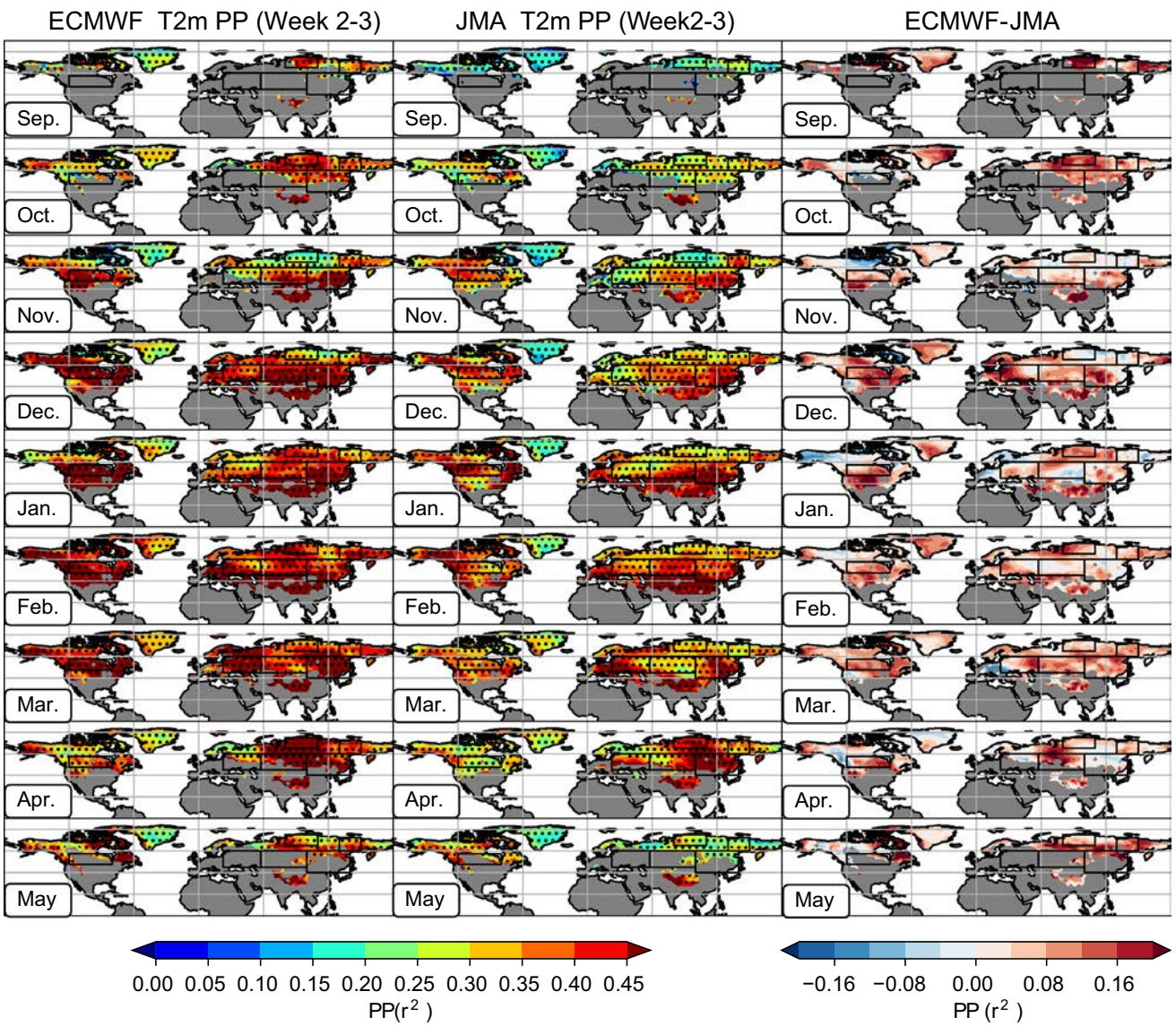

Fig. 11 The potential predictability of SAT assessed by squared Pearson correlation coefficients for Week 2–3 averages for the (left) ECMWF and (middle) JMA models. (right) Differences in the potential predictability between the ECMWF and JMA reforecasts from close initial dates. The stippling in the left and middle panels indicates statistically significant regions based on the bootstrap method (5,000 times resampling)

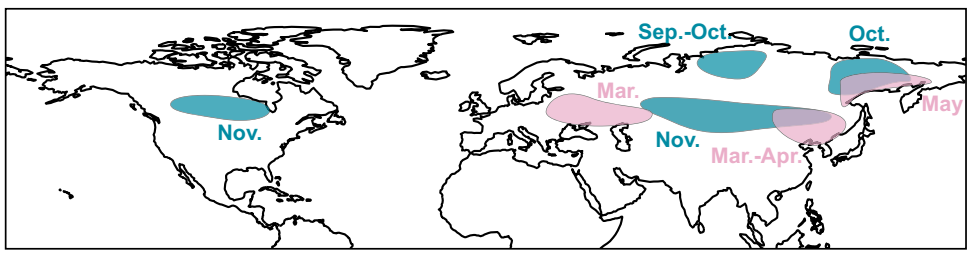

Fig. 12 The cold spots regions and seasons identified in this study. Light pink and light blue colour regions are cold spots in spring and autumn, respectively

analysis, namely no need for extensive model simulations, and frequent reforecasts of the S2S models, enabled us to describe the seasonal change of the snow–SAT interaction in more detail. It should be noted that this study focused on the sub-monthly timescale. Previous studies suggested longer time scale interactions that can offer sub-seasonal and longer timescale predictability. The results obtained in this study do not undermine the suggested longer time scale

interactions through the snow hydrological effect, irrespective of no detection of cold spots by longer time scale interactions. The atmospheric responses to land snow conditions on such time scales are still not well understood due to its poor or diverse representation in climate models (e.g., Henderson et al. 2018). The Liang–Kleeman information flow analysis for the longer time scale variability may contribute to corroborating causal relations of the snow–atmosphere interactions on a longer time scale.

It is worth discussing the underlying mechanisms for the cold spots identified in this study. Previous studies suggested that the coupling strength is strong in the snow melting season (e.g., Xu and Dirmeyer 2011). For instance, Xu and Dirmeyer (2013) found a strong snow–albedo effect in Eastern Europe, the Tibetan Plateau, and the middle latitudes of North America in March (Fig. 5 of Xu and Dirmeyer 2013), which roughly collocate with the cold spots identified in this study (Figs. 4 and 12). Thus, the snow–albedo feedback is active in the cold spots of Eastern Europe in March, and East Asia in March and April. In addition, the cold spots identified around Eastern Europe in March and East Asia in April collocate with the regions of the snow hydrological effect identified by Xu and Dirmeyer (2013b), implying that the snow hydrological effect also plays a role in these regions.

Furthermore, we diagnosed the causality in multiple S2S prediction models. We found that the ECMWF and CMA models generally capture the observed causal relationship, while there are some notable differences among models. All the models analysed in this study, in particular the JMA model, underestimate the influence of SC on SAT (causality from SC to SAT). This result implies the deficiencies of the snow–SAT interaction in the S2S models. We also confirmed similar characteristics in the analysis of SWE. A more detailed analysis using land-related variables, surface heat and radiation fluxes is expected to underpin physical processes that explain the underestimation of the snow influence.

Additionally, we discussed the potential influence of the SC causality difference on the potential predictability of SAT. The higher SAT potential predictability and prediction skill (correlation coefficients) in the ECMWF model than in the JMA model over the SC cold spots is likely to reflect the stronger SC influence on SAT. Note that the potential predictability of SAT also depends on other factors such as soil moisture, sea surface temperature, and sea ice. Therefore, by comparing the potential predictability or prediction skill in different models, we cannot ascertain the role of snow for SAT predictability. However, we consider that the good correspondence between the model differences in the potential predictability of SAT (Fig. 11) and the causality (influence of SC on SAT; Figs. 5 and 6) over the cold spots suggest the snow contribution to the sub-seasonal predictability and prediction skill to some extent.

In this study, we utilized reanalysis datasets from MERRA-2 and ERA5. A prior investigation by Mortimer et al. (2020) assessed the quality of satellite analysis data from GlobSnow v2.0 and reanalyses from ERA-5 and MERRA-2 against ground observations, revealing that the quality of the reanalysis products is on par with that of the satellite product. Nonetheless, relatively large difference between satellite and reanalysis products were observed, indicating the uncertainty in these analysis products. One limitation of our study is the reliance on the quality of the input analysis data. An alternative approach could involve comparing model results with ground observations, although this poses challenges due to differences in spatial scale and the limited availability of ground observations (Komatsu et al. 2023). More effort to evaluation of the reanalysis and model data against independent snow observation is expected to lead to our improved understanding of the snow effect.

This study analysed the SC–SAT causal relation in recent decades. Climate change in the future is likely to modulate the SC–SAT interaction in terms of location and timing on a sub-seasonal timescale, in turn, it will modulate the snow impacts on sub-seasonal SAT predictability. How snow-related predictability alters in changing climate is deserved for future study.

This study renews our understanding of the snow-atmosphere interaction and sub-seasonal predictability arising from SC conditions. This study demonstrated the new alternative and tractable way to diagnose the model behaviours of the snow–atmosphere interaction without sensitivity model experiments. The new analysis method also offers valuable insights into models' shortcomings. Therefore, the diagnostics of this study are useful in the future improvement of S2S prediction.

Supplementary Information The online version contains supplementary material available at https://doi.org/10.1007/s00382-024-07112-6.

Funding This work was supported by the Arctic Challenge for Sustainability II (ArCS II) program (Grant number JPMXD1420318865), the MEXT Program for advanced studies of climate change projection (SENTAN) (Grant Numbers JPMXD0722680734 and JPMXD0722680395), JSPS KAKENHI Grant Number JP23H00351, and the Environment Research and Technology Development Fund (Grant Number JPMEERF20222002) of the Environmental Restoration and Conservation Agency of Japan.

Data availability MERRA-2 data were downloaded from the NASA Goddard Earth Sciences Data and Information Services Center at https://doi.org/https://doi.org/10.5067/9SC1VNTWGWV3, https://doi.org/https://doi.org/10.5067/RKPHT8KC1Y1T, and https://doi.org/https://doi.org/10.5067/OU3HJDS973O0. ERA5 data were downloaded from the Copernicus Climate Data store, https://cds.climate.copernicus.eu. The reforecast data of the CMA, ECMWF, and JMA

models were downloaded from the S2S project website hosted by ECMWF (https://apps.ecmwf.int/datasets/data/s2s/).

Declarations

Conflict of interests The authors have no relevant financial or non-financial interests to disclose.

References

Ambadan JT, Berg AA, Merryfield WJ, Lee W-S (2018) Influence of snowmelt on soil moisture and on near surface air temperature during winter–spring transition season. Clim Dyn 51:1295–1309. https://doi.org/10.1007/s00382-017-3955-8

Ardilouze C, Batté L, Bunzel F et al (2017) Multi-model assessment of the impact of soil moisture initialization on mid-latitude summer predictability. Clim Dyn 49:3959–3974. https://doi.org/10.1007/s00382-017-3555-7

Arduini G, Balsamo G, Dutra E et al (2019) Impact of a multi-layer snow scheme on near-surface weather forecasts. J Adv Modelling Earth Syst 11:4687–4710. https://doi.org/10.1029/2019MS001725

Bai C, Zhang R, Bao S et al (2018) Forecasting the tropical cyclone genesis over the northwest pacific through identifying the causal factors in cyclone-climate interactions. J Atmos Ocean Technol 35:247–259. https://doi.org/10.1175/JTECH-D-17-0109.1

Balsamo G, Beljaars A, Scipal K et al (2009) A revised hydrology for the ecmwf model: verification from field site to terrestrial water storage and impact in the integrated forecast system. J Hydrometeorol 10:623–643. https://doi.org/10.1175/2008JHM1068.1

Cohen J, Entekhabi D (1999) Eurasian snow cover variability and northern hemisphere climate predictability. Geophys Res Lett 26:345–348. https://doi.org/10.1029/1998GL900321

Cohen J, Rind D (1991) The effect of snow cover on the climate. J Clim 4:689–706. https://doi.org/10.1175/1520-0442(1991)004%3c0689:TEOSCO%3e2.0.CO;2

Cook BI, Bonan GB, Levis S, Epstein HE (2008) The thermoinsulation effect of snow cover within a climate model. Clim Dyn 31:107–124. https://doi.org/10.1007/s00382-007-0341-y

Davis RE, Lowit MB, Knappenberger PC, Legates DR (1999) A climatology of snowfall-temperature relationships in Canada. J Geophys Res 104:11985–11994. https://doi.org/10.1029/1999JD900104

de Rosnay P, Balsamo G, Albergel C et al (2014) Initialisation of land surface variables for numerical weather prediction. Surv Geophys 35:607–621. https://doi.org/10.1007/s10712-012-9207-x

Dirmeyer PA (2011) The terrestrial segment of soil moisture–climate coupling. Geophys Res Lett: https://doi.org/10.1029/2011GL048268

Dirmeyer PA, Wang Z, Mbuh MJ, Norton HE (2014) Intensified land surface control on boundary layer growth in a changing climate. Geophys Res Lett 41:1290–1294. https://doi.org/10.1002/2013GL058826

Diro GT, Lin H (2020) Subseasonal forecast skill of snow water equivalent and its link with temperature in selected SubX models. Weather Forecast 35:273–284. https://doi.org/10.1175/WAF-D-19-0074.1

Docquier D, Vannitsem S, Ragone F et al (2022) Causal links between arctic sea ice and its potential drivers based on the rate of information transfer. Geophys Res Lett 49:e2021GL095892. https://doi.org/10.1029/2021GL095892

Douville H (2010) Relative contribution of soil moisture and snow mass to seasonal climate predictability: a pilot study. Clim Dyn 34:797–818. https://doi.org/10.1007/s00382-008-0508-1

Dutra E, Balsamo G, Viterbo P et al (2010) An improved snow scheme for the ECMWF land surface model: description and offline validation. J Hydrometeorol 11:899–916. https://doi.org/10.1175/2010JHM1249.1

Dutra E, Schär C, Viterbo P, Miranda PMA (2011) Land-atmosphere coupling associated with snow cover. Geophys Res Lett. https://doi.org/10.1029/2011GL048435

Estilow TW, Young AH, Robinson DA (2015) A long-term Northern Hemisphere snow cover extent data record for climate studies and monitoring. Earth Syst Sci Data 7:137–142. https://doi.org/10.5194/essd-7-137-2015

Flanner MG, Shell KM, Barlage M et al (2011) Radiative forcing and albedo feedback from the Northern Hemisphere cryosphere between 1979 and 2008. Nat Geosci 4:151–155. https://doi.org/10.1038/ngeo1062

Ganeshi NG, Mujumdar M, Takaya Y et al (2023) Soil moisture revamps the temperature extremes in a warming climate over India. NPJ Clim Atmos Sci 6:12. https://doi.org/10.1038/s41612-023-00334-1

Gelaro R, McCarty W, Suárez MJ et al (2017) The Modern-era retrospective analysis for research and applications, version 2 (MERRA-2). J Clim 30:5419–5454. https://doi.org/10.1175/JCLI-D-16-0758.1

Gichamo TZ, Draper CS (2022) An optimal interpolation–based snow data assimilation for NOAA's Unified Forecast System (UFS). Wea Forecasting 37:2209–2221. https://doi.org/10.1175/WAF-D-22-0061.1

Hall DK, Riggs GA (2021) MODIS/Terra Snow Cover Monthly L3 Global 0.05Deg CMG, Version 61. Boulder, Colorado USA. NASA National Snow and Ice Data Center Distributed Active Archive Center. https://doi.org/10.5067/MODIS/MOD10CM.061

Henderson GR, Peings Y, Furtado JC, Kushner PJ (2018) Snow–atmosphere coupling in the Northern Hemisphere. Nat Clim Chang 8:954–963. https://doi.org/10.1038/s41558-018-0295-6

Hersbach H, Bell B, Berrisford P et al (2020) The ERA5 global reanalysis. Quart J Roy Meteor Soc 146:1999–2049. https://doi.org/10.1002/qj.3803

Hirai M, Sakashita T, Kitagawa H et al (2007) Development and validation of a new land surface model for jma's operational global model using the CEOP observation dataset. J Meteorol Soc Japan 85A:1–24. https://doi.org/10.2151/jmsj.85A.1

Japan Meteorological Agency (2023) Outline of the operational numerical weather prediction at the Japan Meteorological Agency. https://www.jma.go.jp/jma/jma-eng/jma-center/nwp/outline2023-nwp/pdf/outline2023_all.pdf Accessed on 27 July 2023.

Jeong J-H, Linderholm HW, Woo S-H et al (2013) Impacts of snow initialization on subseasonal forecasts of surface air temperature for the cold season. J Clim 26:1956–1972. https://doi.org/10.1175/JCLI-D-12-00159.1

Jiang S, Hu H, Zhang N et al (2019) Multi-source forcing effects analysis using Liang-Kleeman information flow method and the community atmosphere model (CAM4.0). Clim Dyn 53:6035–6053. https://doi.org/10.1007/s00382-019-04914-x

Kolstad EW (2017) Causal pathways for temperature predictability from snow depth. J Clim 30:9651–9663. https://doi.org/10.1175/JCLI-D-17-0280.1

Komatsu KK, Takaya Y, Toyoda T, Hasumi H (2023) A submonthly scale causal relation between snow cover and surface air temperature over the autumnal eurasian continent. J Clim 36:4863–4877. https://doi.org/10.1175/JCLI-D-22-0827.1

Koster RD, Suarez MJ, Ducharne A et al (2000) A catchment-based approach to modeling land surface processes in a general circulation model: 1 Model Structure. J Geophys Res 105:24809–24822. https://doi.org/10.1029/2000JD900327

Koster RD, Mahanama SPP, Yamada TJ et al (2011) The second phase of the global land-atmosphere coupling experiment: soil moisture

contributions to subseasonal forecast skill. J Hydrometeorol 12:805–822. https://doi.org/10.1175/2011JHM1365.1
Kumar A, Yang F (2003) Comparative influence of snow and SST variability on extratropical climate in Northern Winter. J Clim 16:2248–2261. https://doi.org/10.1175/2771.1
Li F, Orsolini YJ, Keenlyside N et al (2019) Impact of snow initialization in subseasonal-to-seasonal winter forecasts with the Norwegian climate prediction model. J Geophys Res 124:10033–10048. https://doi.org/10.1029/2019JD030903
Li W, Hu S, Hsu P-C et al (2020) Systematic bias of Tibetan Plateau snow cover in subseasonal-to-seasonal models. Cryosphere 14:3565–3579. https://doi.org/10.5194/tc-14-3565-2020
Liang XS (2008) Information flow within stochastic dynamical systems. Phys Rev E 78:031113. https://doi.org/10.1103/PhysRevE.78.031113
Liang XS (2013) The Liang-Kleeman information flow: theory and applications. Entropy 15:327–360. https://doi.org/10.3390/e15010327
Liang XS (2014) Unraveling the cause-effect relation between time series. Phys Rev E 90:52150. https://doi.org/10.1103/PhysRevE.90.052150
Liang XS (2015) Normalizing the causality between time series. Phys Rev E 92:22126. https://doi.org/10.1103/PhysRevE.92.022126
Liang XS, Kleeman R (2005) Information transfer between dynamical system components. Phys Rev Lett 95:244101. https://doi.org/10.1103/PhysRevLett.95.244101
Lin P, Wei J, Yang Z-L et al (2016) Snow data assimilation-constrained land initialization improves seasonal temperature prediction. Geophys Res Lett 43:11. https://doi.org/10.1002/2016GL070966
Liu J, Pu Z (2019) Does soil moisture have an influence on near-surface temperature? J Geophys Res 124:6444–6466. https://doi.org/10.1029/2018JD029750
McGraw MC, Barnes EA (2018) Memory matters: a case for granger causality in climate variability studies. J Clim 31:3289–3300. https://doi.org/10.1175/JCLI-D-17-0334.1
Mortimer C, Mudryk L, Derksen C et al (2020) Evaluation of long-term Northern Hemisphere snow water equivalent products. Cryosphere 14:1579–1594. https://doi.org/10.5194/tc-14-1579-2020
Orsolini YJ, Senan R, Balsamo G et al (2013) Impact of snow initialization on sub-seasonal forecasts. Clim Dyn 41:1969–1982. https://doi.org/10.1007/s00382-013-1782-0
Orsolini YJ, Senan R, Vitart F et al (2016) Influence of the Eurasian snow on the negative North Atlantic Oscillation in subseasonal forecasts of the cold winter 2009/2010. Clim Dyn 47:1325–1334. https://doi.org/10.1007/s00382-015-2903-8
Orsolini Y, Wegmann M, Dutra E et al (2019) Evaluation of snow depth and snow cover over the Tibetan Plateau in global reanalyses using in situ and satellite remote sensing observations. Cryosphere 13:2221–2239. https://doi.org/10.5194/tc-13-2221-2019
Pegion K, Kirtman BP, Becker E et al (2019) The subseasonal experiment (SubX): a multimodel subseasonal prediction experiment. Bull Am Meteorol Soc 100:2043–2060. https://doi.org/10.1175/BAMS-D-18-0270.1
Peings Y, Douville H, Alkama R, Decharme B (2011) Snow contribution to springtime atmospheric predictability over the second half of the twentieth century. Clim Dyn 37:985–1004. https://doi.org/10.1007/s00382-010-0884-1
Pullen S, Jones C, Rooney G (2011) Using satellite-derived snow cover data to implement a snow analysis in the met office global NWP model. J Appl Meteorol Climatol 50:958–973. https://doi.org/10.1175/2010JAMC2527.1
Reichle RH, Koster RD, De LGJM et al (2011) Assessment and enhancement of MERRA land surface hydrology estimates. J Clim 24:6322–6338. https://doi.org/10.1175/JCLI-D-10-05033.1
Reichle RH, Draper CS, Liu Q et al (2017) Assessment of MERRA-2 land surface hydrology estimates. J Clim 30:2937–2960. https://doi.org/10.1175/JCLI-D-16-0720.1
Ruggieri P, Benassi M, Materia S et al (2022) On the role of Eurasian autumn snow cover in dynamical seasonal predictions. Clim Dyn 58:2031–2045. https://doi.org/10.1007/s00382-021-06016-z
Saha SK, Sujith K, Pokhrel S et al (2017) Effects of multilayer snow scheme on the simulation of snow: offline Noah and coupled with NCEP CFSv2. J Adv Model Earth Syst 9:271–290. https://doi.org/10.1002/2016MS000845
Stieglitz M, Ducharne A, Koster R, Suarez M (2001) The impact of detailed snow physics on the simulation of snow cover and subsurface thermodynamics at continental scales. J Hydrometeorol 2:228–242. https://doi.org/10.1175/1525-7541(2001)002%3c0228:TIODSP%3e2.0.CO;2
Takaya Y, Kosaka Y, Watanabe M, Maeda S (2021) Skilful predictions of the Asian summer monsoon one year ahead. Nat Commun 12:2094. https://doi.org/10.1038/s41467-021-22299-6
Thomas JA, Berg AA, Merryfield WJ (2016) Influence of snow and soil moisture initialization on sub-seasonal predictability and forecast skill in boreal spring. Clim Dyn 47:49–65. https://doi.org/10.1007/s00382-015-2821-9
Vannitsem S, Liang XS (2022) Dynamical dependencies at monthly and interannual time scales in the climate system: study of the north pacific and atlantic regions. Tellus A. https://doi.org/10.16993/tellusa.44
Vitart F, Ardilouze C, Bonet A et al (2017) The subseasonal to seasonal (S2S) prediction project database. Bull Am Meteorol Soc 98:163–173. https://doi.org/10.1175/BAMS-D-16-0017.1
Walters D, Baran AJ, Boutle I et al (2019) The met office unified model global atmosphere 7.0/7.1 and JULES global land 7.0 configurations. Geosci Model Dev 12:1909–1963. https://doi.org/10.5194/gmd-12-1909-2019
Wu R, Kirtman BP (2007) Observed relationship of spring and summer east asian rainfall with winter and spring Eurasian snow. J Clim 20:1285–1304. https://doi.org/10.1175/JCLI4068.1
Xu L, Dirmeyer P (2011) Snow-atmosphere coupling strength in a global atmospheric model. Geophys Res Lett. https://doi.org/10.1029/2011GL048049
Xu L, Dirmeyer P (2013) Snow-atmosphere coupling strength. part II: Albedo effect versus hydrological effect. J Hydrometeorol 14:404–418. https://doi.org/10.1175/JHM-D-11-0103.1
Xue Y, Yao T, Boone AA et al (2021) Impact of initialized land surface temperature and snowpack on subseasonal to seasonal prediction project, phase I (LS4P-I): organization and experimental design. Geosci Model Dev 14:4465–4494. https://doi.org/10.5194/gmd-14-4465-2021
Yasunari T, Kitoh A, Tokioka T (1991) Local and remote responses to excessive snow mass over Eurasia appearing in the northern spring and summer climate. J Meteorol Soc Japan Ser II 69:473–487. https://doi.org/10.2151/jmsj1965.69.4_473
Yonehara H, Matsukawa C, Nabetani T, et al (2020) Upgrade of JMA's operational global model. WGNE Research Activities in Earth System Modelling 6:6–19. https://wgne.net/bluebook/uploads/2020/docs/06_YONEHARA_Hitoshi_UpgradeOfGSM.pdf.
Zhang T (2005) Influence of the seasonal snow cover on the ground thermal regime: an overview. Rev Geophys. https://doi.org/10.1029/2004RG000157